# Experimental Validation of Numerical Model for Turbulent Flow in a Tangentially Fired Boiler with Platen Reheaters

**Chang Hao Zheng, Xu Chang Xu**
*State Key Laboratory of Coal Clean Combustion, Tsinghua University, Beijing, China 100084*
**Jong Wook Choi***
*School of Mechanical and Automotive Engineering, Sunchon National University, Suncheon, Chonnam 540-742, Korea*

A 1 : 20 laboratory scale test rig of a 200 MW tangentially fired boiler is built up with completely simulated structures such as platen heaters and burners. Iso-thermal turbulent flow in the boiler is mapped by 3-D PDA (Particle Dynamic Analyzer). The 3-D numerical models for the same case are proposed based on the solution of $k$-$\varepsilon$ model closed RANS (Reynolds time-Averaged Navier-Stokes) equations, which are written in the framework of general coordinates and discretized in the corresponding body-fitted meshes. Not only are the grid lines arranged to fit the inner/outer boundaries, but also to align with the streamlines to the best possibility in order to reduce the NDE (numerical diffusion errors). Extensive comparisons of profiles of mean velocities are carried out between experiment and calculation. Predicted velocities in burner region were quantitatively similar with measured ones, while those in other area have same tendency with experimental counterpart.

**Key Words :** Tangentially Fired Boiler, Turbulent Flow, PDA (Particle Dynamic Analyzer), General Coordinates, NDE (Numerical Diffusion Error)

## Nomenclature

$\tilde{B}^{ii}$: Discretized metric components
$\mathbf{g}^i$ : Contravariant base vector
$\mathbf{I}_j$ : Base vector of Cartisian coordinates
$\mathbf{i}$ : Unit vector
$J$ : Jacobian of the transformation
$k$ : Turbulent kinetic energy
$N$ : Total number of particles
$p$ : Pressure
$p^k$ : Control function
r : Position vector
$\Delta t$: Time step
$\bar{U}$ : Mean velocity of particles
$U$ : Velocity of a particle
$u_j$ : Velocity component in the fixed Cartesian coordinates
$V^i$: Contravariant velocity component in the curvilinear coordinates
$x_i$ : Cartesian coordinates

**Greek symbols**

$\varepsilon$ : Turbulence dissipation rate
$\mu$ : Coefficient of viscosity
$\rho$ : Density of glass beans
$\xi^i$ : General coordinates
$\Delta\xi$: Distance between the nodes

* Corresponding Author,
**E-mail** : choijw99@postown.net
**TEL** : +82-61-750-3957; **FAX** : +82-61-753-3962
School of Mechanical and Automotive Engineering, Sunchon National University, Suncheon, Chonnam 540-742, Korea. (Manuscript **Received** May 10, 2002; **Revised** October 23, 2002)

## 1. Introduction

The popularity of a TFB (Tangentially Fired Boiler) in power industry is due to its remarkable advantages such as suitability to various types of coal, easy ignition and flame stability. However, the problems such as GSEI (Gas-Side-Energy-Imbalance), erosion and slagging are becoming

more and more serious with the increase of the capacity of the boiler, and partially offset the enhanced efficiency resulted from the raised operational parameters.

Numerical investigation is highly expected to provide a detailed knowledge helpful to solve the problems, and much projects of such topics were carried out in recent years, e.g., Smoot and Pratt (1979), Honney and Kent (1989), Luo et al. (1991), Sandro (2000), Fan et al. (2001). Those numerical models are generally based on the flow field modeled by the solution of RANS (Reynolds time-Averaged Navier-Stokes) equations closed by turbulence model methods, and coupled with other sub-models describing concerned physical or chemical phenomenon such as gas phase reaction, radiation and coal-particle dynamics, combustion and radiation. It is evident that the aerodynamic simulation plays the key role in the whole process. As a result, its accuracy and boundary conditions are crucial to the interested predictions.

Most previous models as mentioned were discretized and solved on Cartesian coordinates and corresponding orthogonal meshes with the grid lines parallel to the furnace boundaries. Because the jets from corner-positioned burner are highly deviated from the grid lines, well-known NDE (Numerical Diffusion Error) could not be avoided and may damage the accuracy seriously. Though the attentions were being paid on the calculation while various methods were being tried, more attempts are still welcomed, since it is not a trifle mission to consider the NDE in the engineering cases with the complex flow pattern in 3-D geometrical domain. On the other hand, it is necessary to consider the structure of the platen heater/reheater in the modeling, especially when the study is focused on describing such phenomenon as the GSEI, which is taken place on top of the furnace and is affected by the existence of heating devices there. Unfortunately, much previous studies omitted or simplified the structures for the convenience of treating boundary conditions.

Finally, the measurement of turbulent flow in a TFB model is necessary to the validation of numerical model and it was seldom done before with the 3D-PDA, a sophisticated and advanced devices based on a phase Doppler anemometer, with which more accurate and comprehensive measurement can be expected. In the present study, a 200MW TFB has been carefully modeled both experimentally and computationally. Detailed comparison is made between experiment and calculation in order to assess the efficiency of the proposed numerical model.

## 2. Experimental

### 2.1 Test facility

A 1 : 20 model of a 200MW boiler furnace was built (Su, 1999). The model has the cross-section of 683×583 mm, and the height of 2208 mm as shown in Fig. 1. The side walls were made up of the plate-glasses. A set of aluminum plates fixed on the upper furnace represented plate-heaters. Two groups of burners were positioned at each corner and were directed at 38.5° and 45.8° to the wall. Each group comprised of four primary-air burners sandwiched by two secondary-air ones, and the upper group had an additional tertiary-

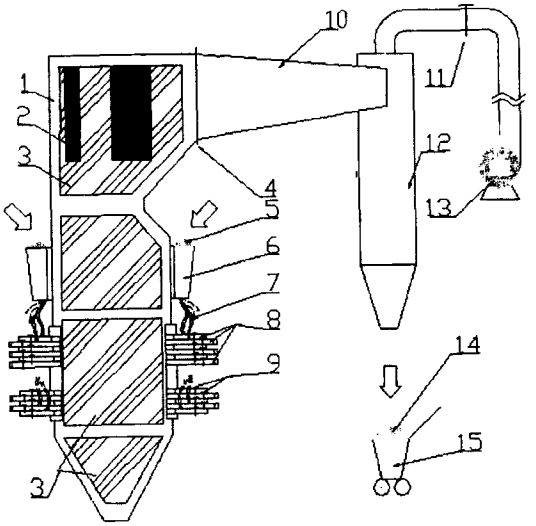


1. furnace, 2. plate heaters, 3. plane-glasses. 4. honeycomb, 5. tracer, 6. tracer storage, 7. hoses, 8. entrance duct, 9. venturi throat, 10. contraction, 11. throttle valves, 12. cyclone separator and filter system, 13. exhaust blower, 14. tracer, 15. collection bucket

**Fig. 1** Schematic diagram of TFB boiler model

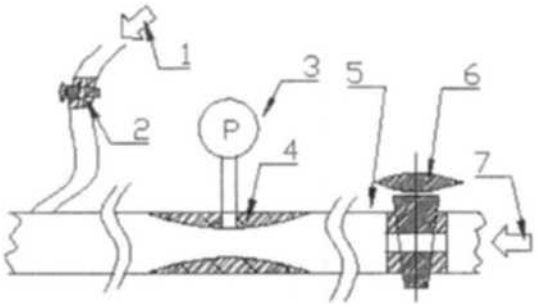


1. tracers, 2. throttle valves, 3. pressure meters, 4. Venturi throat, 5. square duct, 6. throttle valves, 7. air

**Fig. 2** Schematic diagram of entrance duct

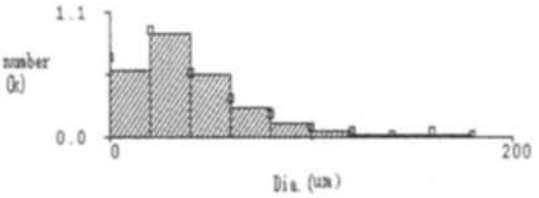


**Fig. 3** Size distribution of the glass beans

air burner at the top. The burner was simulated by a square-section duct, which has a venturi throat and a particle-feeding bypass for primary burner as shown in Fig. 2. A honeycomb positioned at the exit of the furnace simulated the impact of the heaters (in horizontal flue of a real boiler) on the aerodynamic character near the exit.

Air was induced into the furnace by the exhaust-blower, and the primary, secondary and tertiary air velocities were set as 17, 25 and 30 m/s, respectively. The glass beans ($\rho$=2990 kg/m$^3$) with the size distribution as shown in Fig. 3 were introduced into the air with the total mass flow rate of about 5 kg/h.

### 2.2 Measurement instrumentation

Velocity measurement was made with the 3D-PDA (3D-Particle Dynamic Analyzer) developed by DENTEC, which is a three-color phase-Doppler anemometer (Choi et al., 2002). It can measure the velocity and the size of the spherical particle simultaneously. A power-adjustable argon-ion laser source was used with the maximum power of 5 W. The optics arrangement with three colors-six beams was introduced to measure three components of the particle velocity. The 40 MHz frequency shift was made by Braggcell for one of two beams with same color.

### 2.3 Measurement and uncertainty

Five horizontal planes were selected for the measurement. Three of them were in the port region, where intensive mixing happens and numerical diffusion is liable to appear in the calculation. The other two planes were in further downstream. One vertical plane at the exit of furnace was also measured, where the velocity is spatially non-uniform which is related to the GSEI. The uniform grids with 12×18 nodes were used in measurement. At the typical sampling rate of 0.2-1 kHz, 3000 validated data were collected at each node. The range of the phase angle is validated in case the sum of the phase angles should not be greater than 15 degree.

The velocities of the particles less than 9 $\mu$m were considered to be equal to those of the gas. The error come from this assumption would be neglectable, since the relaxation time scale (about $10^{-4}$s) for the attitude of the particle dispersion is small enough even compared with turbulent time scale (about $10^{-2}$s). The well-known uncertainty in the statistical process is called 'biased errors' (Adrian and Yao, 1987), which comes from the non-uniformly distributed velocity samples. The interval-time weighted method was used to reduce such error in the present study.

$$\bar{U}_J=\frac{\sum_{i=1}^{N}U_J\Delta t_i}{\sum_{i=1}^{N}\Delta t_i} \tag{1}$$

$$\sqrt{\bar{u}_J^2}=\left[\frac{\sum_{i=1}^{N}(U_{J,i}-\bar{U}_J)^2\Delta t_i}{\sum_{i=1}^{N}\Delta t_i}\right]^{1/2} \tag{2}$$

The total error was expected not to exceed 5% by Eq. (1) for mean velocities and 10% by Eq. (2) for root mean square fluctuations, respectively.

## 3. Computation

### 3.1 Mathematical formulation

Continuity equation can be expressed in terms of primitive variables as Eq. (3).

$$\frac{\partial}{\partial \xi^i}\left(\frac{\rho V^i}{J}\right)=0 \tag{3}$$

where, J is the Jacobian of the transformation as Eq. (4).

$$\frac{1}{J}=\frac{\partial(x_1, x_2, x_3)}{\partial(\xi^1, \xi^2, \xi^3)} \tag{4}$$

The momentum equation expressed in the strong conservative form (Yang et al., 1994) in the general coordinate system is selected. It can be written in terms of primitive variables as Eq. (5).

$$\frac{\partial}{\partial \xi^i}\left(\frac{\rho V^i}{J}u_j\right)=\frac{\partial}{\partial \xi^i}\left(\mu\frac{\mathbf{g}^i\cdot\mathbf{g}^k}{J}\frac{\partial u_j}{\partial \xi^k}\right)-I_j\cdot\frac{\mathbf{g}^i}{J}\frac{\partial p}{\partial \xi^i} \tag{5}$$

where $V^i=\mathbf{g}^i\cdot\mathbf{V}$ is contravariant velocity component in the curvilinear coordinate.

The turbulence kinetic k and its dissipation rate $\varepsilon$ are governed by Eqs. (6) and (7) in terms of primitive variables.

$$\frac{\partial}{\partial \xi^i}\left(\frac{\rho V^i}{J}k\right)=\frac{\partial}{\partial \xi^i}\left(\frac{\mu}{\sigma_k}\frac{\mathbf{g}^i\cdot\mathbf{g}^k}{J}\cdot\frac{\partial k}{\partial \xi^j}\right)+\frac{1}{J}(G-\rho\varepsilon) \tag{6}$$

$$\frac{\partial}{\partial \xi^i}\left(\frac{\rho V^i}{J}\varepsilon\right)=\frac{\partial}{\partial \xi^i}\left(\frac{\mu}{\sigma_\varepsilon}\frac{\mathbf{g}^i\cdot\mathbf{g}^k}{J}\cdot\frac{\partial \varepsilon}{\partial \xi^j}\right)+\frac{\varepsilon}{k}(C_{\varepsilon 1}G-C_{\varepsilon 2}\rho\varepsilon)\frac{1}{J} \tag{7}$$

The expression of G and the constants of $C_{\varepsilon 1}$, $C_{\varepsilon 2}$, $\sigma_k$, $\sigma_\varepsilon$ are discussed in other literatures.

### 3.2 Numerical procedure

Equations (3)-(7) are discretized using a finite difference method in the generalized coordinate space, with the metric information expressed in terms of area vectors. The equations are solved on a structured, non-staggered grids. The velocity components in fixed Cartesian directions are treated as scalars after the transformation from physical coordinates to computational space coordinates. To approximate the convection across the cell surfaces, the based EDS (Exponential Differencing Scheme) is used. Cross-derivatives in the momentum equations caused by non-orthogonality are dropped into source terms to retain the diagonal dominance of the matrix. The incompressibility constraint is enforced by the pressure correction methods where the pressure-velocity coupling is handled by SIMPLE-like methods. A generalized wall-boundary approach is used and the velocities and distances in the equation are calculated in the local Cartesian coordinate systems. The governing equations for the scalars and pressure correction equations are solved sequentially in the each outer iteration. A strongly implicit procedure is used to solve the Poisson-like linear systems in the inner iterations.

### 3.3 Special treatments

Special techniques employed in the solution include : Firstly, to take into account the smoothness properties of the coordinate mapping, which appears essential for locally non-smooth meshes (Wesseling et al., 1998). Secondly, the secondary pressure correction method is used as the acceleration means (Ferziger and Peric, 1995). In this method, the commonly neglected cross-direction terms in the transformed pressure correction equation are considered iteratively. It is proved that those terms are essential for the fast convergence especially when the grids are highly non-orthogonal and the number of the nodes is large. Thirdly, the momentum interpolation method (Xu and Zhang, 1998) by Rhie and Chow is extended to the present case with the pressure gradient terms being differentiated in the way that the mass conservation is strictly followed as Eq. (8). It is appeared that pressure oscillations could be safely avoided in the non-staggered meshes due to the reduced discretization error in our scheme.

$$(\tilde{V}^i)_f=(\tilde{V}^{i*})_f-(\tilde{B}^{ii})_f\left(\frac{p_{f+\frac{1}{2}\Delta\xi^i}-p_{f-\frac{1}{2}\Delta\xi^i}}{\Delta\xi^i}\right)+\frac{(\tilde{B}^{ii})_{f+\Delta\xi^i}p_{f+\Delta\xi^i}-(\tilde{B}^{ii})_{f-\Delta\xi^i}p_{f-\Delta\xi^i}}{2\Delta\xi^i} \tag{8}$$

where subscript 'f' refers to a surface. It is shown that those techniques are essential for the accurate and computationally efficient solution of the present case where the grids are locally non-smooth and highly non-orthogonal due to the fact that the grids have been generated to adapt the complex flow patterns to the best possibilities.

### 3.4 Mesh generation

The grid of the furnace of the TFB was generated by numerical solution of the elliptic partial differential equations (Thompson et al., 1985, Kim and Lee, 2002) and by properly specified boundary conditions. In the present study, we employed the Poisson equation with the control function as generation system. Actual computation was done in the transformed region. The corresponding transformed equation is written in the vector form as Eq. (9).

$$g^{ij}\frac{\partial^2 \mathbf{r}}{\partial \xi^i \partial \xi^j}+(g^{kk}p^k)\frac{\partial \mathbf{r}}{\partial \xi^k}=\mathbf{0} \tag{4}$$

where $\mathbf{r}=x_m\mathbf{i}_m$ (summation on the indices).

The control function $p^k$ is designed with exponential functions as Eq. (10).

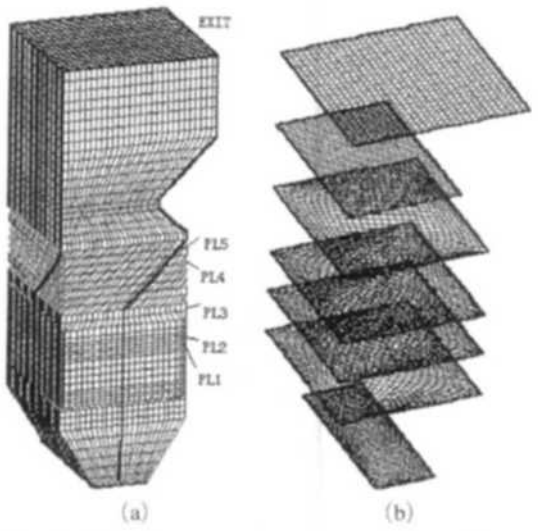


**Fig. 4** 3D grids of boiler and horizontal grids at different planes

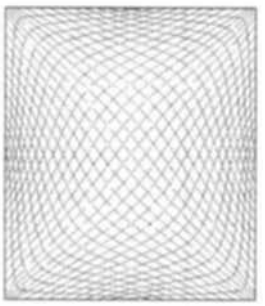

**Fig. 5** Horizontal grid plane at burner region

$$\begin{cases} P^k=-\sum_{l=1}^{n} a_l Sgn(\xi^k-\xi^l)\exp(-b_l T_l) \\ T_l=\sqrt{\sum_{l=1}^{n} C_{lk}(\xi^k-\xi^l)^2} \end{cases} \tag{10}$$

By adjusting the constants of $a_l$, $b_l$, $C_l$ in the Eq. (10), neighboring coordinate lines are attracted to the specified lines $\xi=\xi^l$.

The meshes as shown in Fig. 4(a) were generated to adapt the flow patterns to the best possibilities. In particular, the horizontal grid lines in the burner region were arranged as shown in Fig. 5, where the grid lines near the ports approximate to the diagonals and those around the center approximate to a circle. In the upper part of the furnace, the horizontal grid lines are nearly parallel to the boundaries. In the region between the above two planes, the directions of the horizontal grid lines changed gradually with the height of the plane as shown in Fig. 4(b).

## 4. Results and Discussion

Horizontal velocity vectors at five measurement planes are shown in Fig. 6. At the planes 1 and 2 positioned at two upper primary-air-port regions, the measured velocity vectors show that the jets from the ports shift to the boundary while mixing with the swirl flow in full of the section. This is also evident in the prediction. Generally, there is good agreement between prediction and experiment, except that the directions of some vectors near the middle of the boundary are not align with the measured ones. The skewness of the grid lines and streamlines may account for this. Also, the experimental swirl center in the plane 2 is unaccountably displaced away from the center of the furnace. It is shown that both predicted and measured diameters of tangential circle in the plane 2 are slightly smaller than those in the plane 1. This reason is that the air-supply condition near the corners in the plane 2 is better than that in the plane 1, and thus the driving pressure difference between two sides of each jet flow is smaller in the plane 2, causing less shift to the boundary.

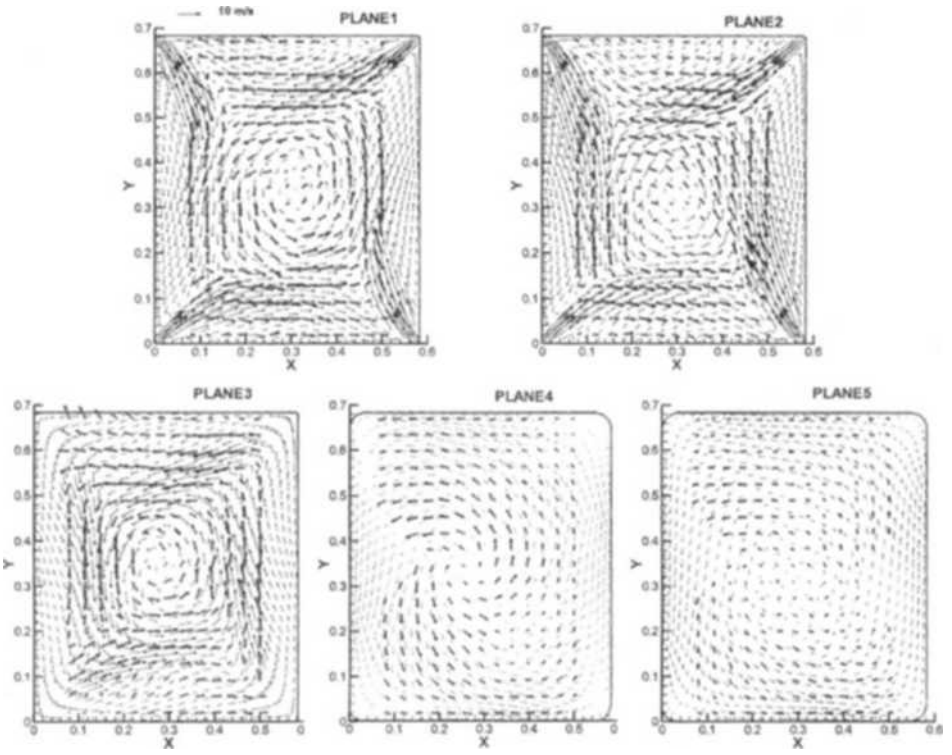


**Fig. 6** Comparisons of velocity vectors for plane 1-plane 5

At locations 4 and 5, further up the furnace, the flow pattern is purely a swirl. It is evident that the swirl velocities decrease gradually as the downstream gas flows of the furnace. The basic similarity between the measurements and predictions is evident in the planes 4, 5. At the plane 3 just positioned above the burner region, the swirl is shown to be at transitional status between jet-forced swirl and free one. Both experiment and calculation agreeably illustrate such feature.

In order to illustrate the dependence of the NDE on the grid pattern as well as the impact of such error on the result in the burner region of the TFB, the contrast numerical experiment was carried out based on the commonly used orthogonal mesh system with the grid lines parallel to the boundaries. Both predictions based on such mesh and those based on the body-fitted mesh are shown in the Fig. 7. For the prediction based on orthogonal grid, the grid lines are obviously deviated from the streamlines near the ports where the gradient of the velocities is steep. In the

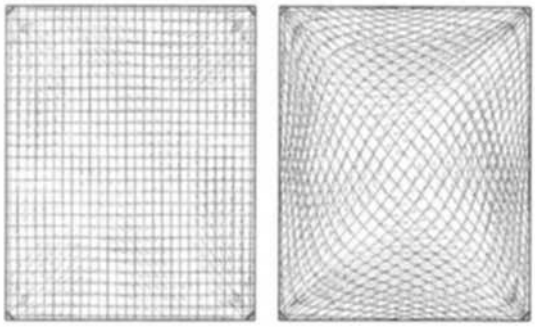

(a) prediction based on orthogonal grid (b) Prediction based on body-fitted grid

**Fig. 7** Predictions for velocity vectors with different grid systems at plane 1

circumstance, the serious NDE appears and is illustrated by unreasonable radial expansion and the rapid slowdown of the jets as they are ejected from the ports into the furnace. On the contrary, for the case of BFG (Body-Fitted Grid), there is not visible impact of the NDE on the flow pattern of the jets, which are ejected from the ports more

tightly and more deeply into the swirl flow. As the prediction is verified below by its comparisons with the experiment, it is concluded that the NDE is kept within limit by employing BFG in the present study while the solution quality has been improved remarkably. The better solution quality is mainly contributed by the alignment of the grid lines on the BFG with the streamlines near the ports as shown in the Fig. 7.

Figures 8-10 give detailed comparisons of measured and predicted mean velocity components at planes 1, 3, and 5, respectively. In the plane 1, both transverse u-component and streamwise w-component are well predicted, compared with measured ones. The main structure of high speed jet in cross-flow is depicted in the profiles of u-components, where the peaks of jet velocity are flattened rapidly before the jet is entirely merged into ambient air near the center line of the plane. The correctly predicted jet direction suggests the effectiveness of grid lines arrangement for reducing the NDE in the present study. The streamwise velocities in the region of the center and the boundary are higher than those in the middle ring due to inflation effect of the jets.

At the plane 3, the transverse velocity components are similar as those at the plane 1, whereas the streamwise velocity components on two planes are quite different. The w-velocity is lower in the center region than that in the middle ring. The adverse pressure gradient, which is caused by the streamwise decay of the swirl, may account for this. However, the w-velocity is overpredicted, especially at the center region. And there is also some discrepancy near the center point of the plane where small peaks of the measured w-ve-

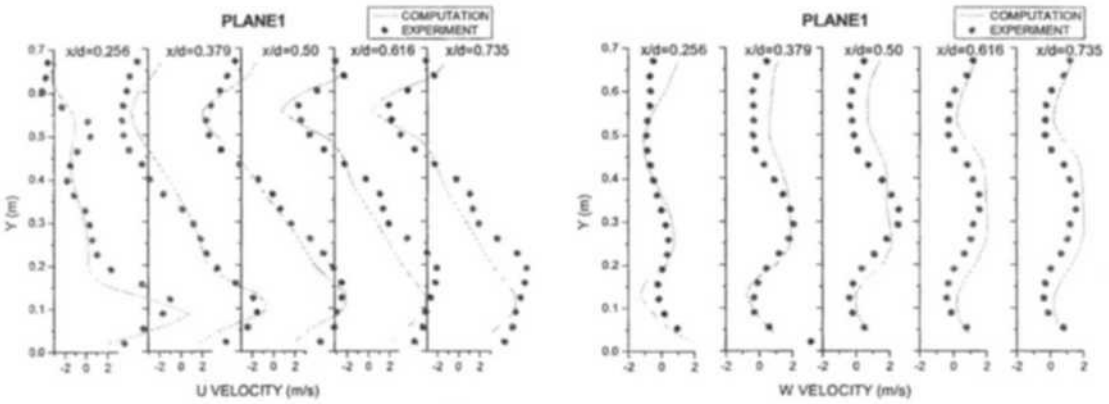


**Fig. 8** Profiles of U and W mean velocity components at five equally spaced stations on the plane 1

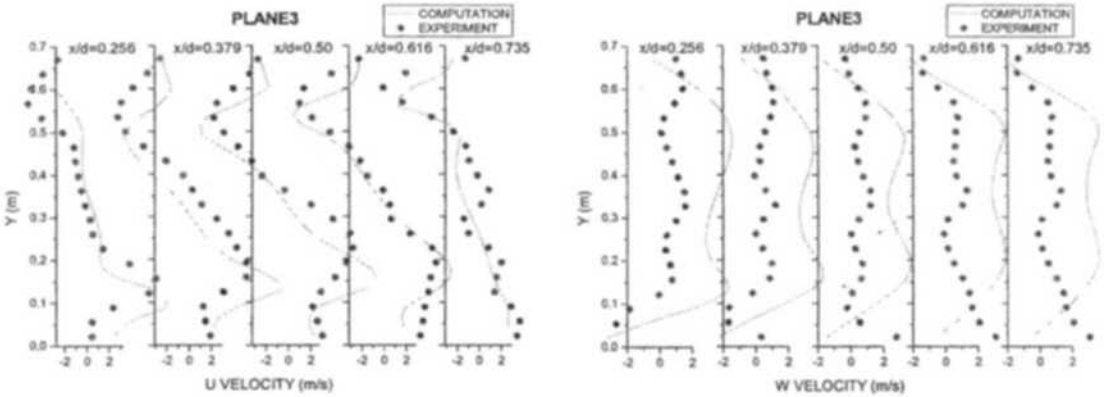


**Fig. 9** Profiles of U and W mean velocity components at five equally spaced stations on the plane 3

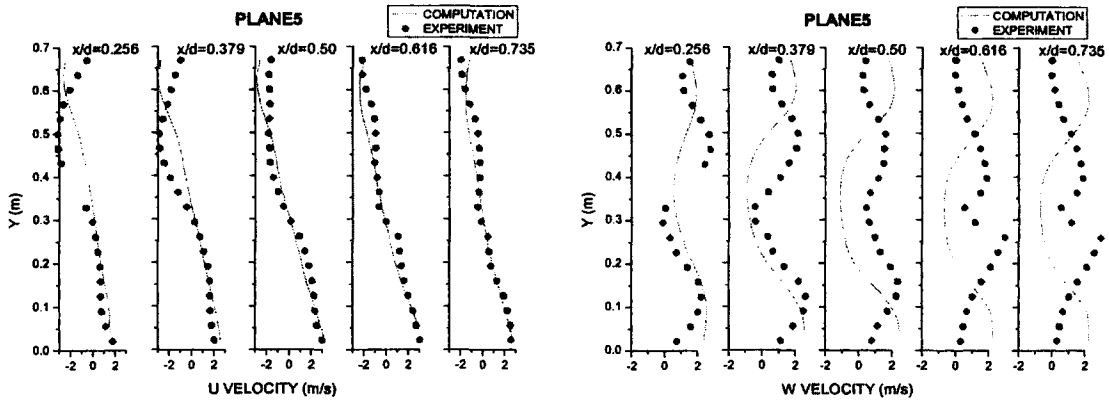


**Fig. 10** Profiles of U and W mean velocity components at five equally spaced stations on the plane 5

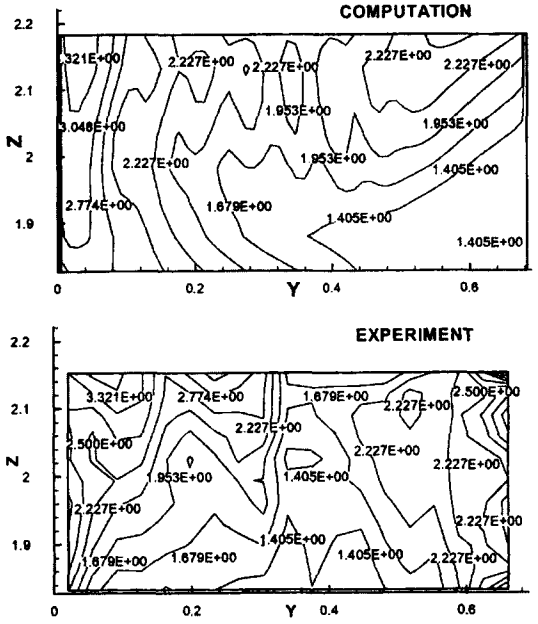


**Fig. 11** Comparison of streamwise velocity components at the exit cross-section

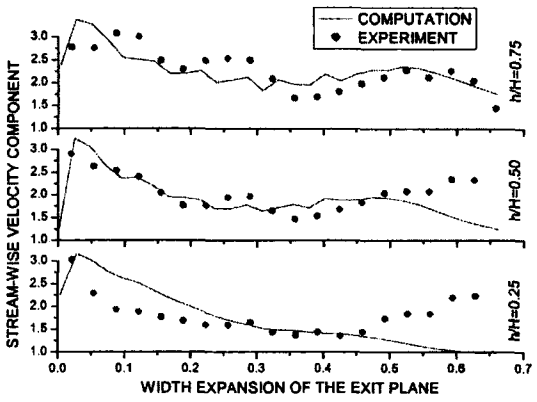


**Fig. 12** Variations of streamwise velocity components at three equally spaced stations at the exit cross-section

locity appear. The discrepancy implies that the turbulent model overestimates the diffusive transport of momentum in the streamwise direction, and cause the flatten velocity distribution.

The predicted swirl velocity components in ane 5 are mainly featured as solid-body-motions, are in general agreement with measured ones, which however show some local free-vortex-motions. The differences between experimental w-velocity components and predicted ones are still evident, with the flattened and enlarged reversal regions in the calculations. Again, the weakness of turbulence model for swirling flow accounts for such defect, which appears to exaggerate solid-body-motion and thus smears out free-vortex motion in reality.

Figure 11 shows the contours of the streamwise components of the velocities at the exit cross-section of the furnace. General agreement is achieved between computations and experiments. The measurements show high velocities near the right-hand side and low velocities near the left of the middle line. The predictions show a similar general pattern except that low velocities are also shown near the right-down corner. The predicted maximum and minimum velocities agree fairly well with the measured ones. Transverse profiles for the streamwise mean velocities as shown in

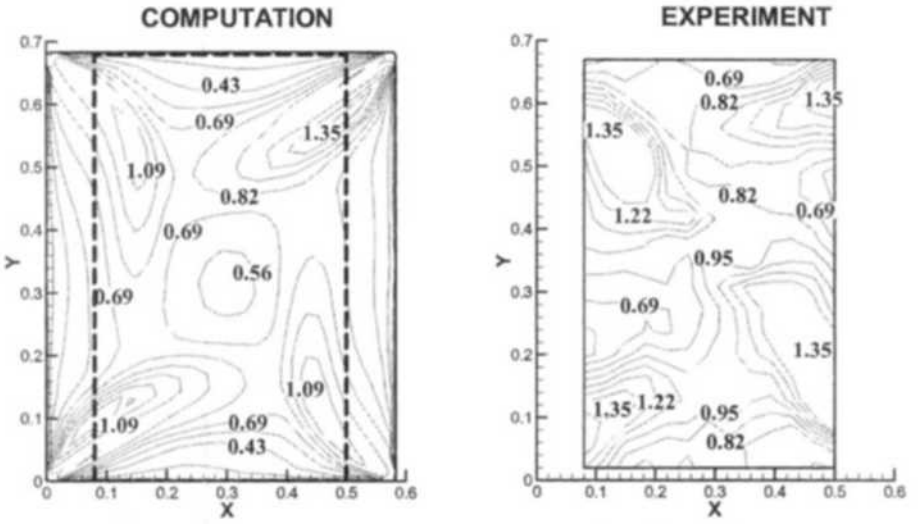


(Area enclosed by broken line box on the left figure corresponds to that to be measured by PDA)

**Fig. 13** Comparison of predicted and measured turbulent kinetic energy normalized by inlet value on plane 1

Fig. 12 further manifest fairly good comparison except some under-predictions near the right-down corner.

Figure 13 shows the distributions of turbulent kinetic energy on the horizontal plane in the burner region. Both results share common features as the high-speed jets from the ports provoke strong turbulent oscillations by impinging and mixing with the low-speed swirl. It is depicted that turbulent kinetic energy is transported and dissipated with the fluid flow from the jets and its distribution largely depend on the pattern of fluid flow, which also emphasizes how important it is to accurately simulate the transportation of fluid flow in this region. The difference lies on the fact that the measured turbulent kinetic energy on the plane 1 is generally higher than the predicted one and its pattern is not so smooth and regular as that of the calculation. The reason for the discrepancy is likely because of the deficiency of k-epsilon turbulent model, which is based on the isotropic assumption of the microscopic eddies for well-developed turbulent flow in the parallel duct. The assumption may not be the case for the turbulent flow in the burner region of the TFB, which is far away from being well-developed and has a large scope of the turbulent scale of the eddies.

## 5. Conclusion

Though it is usual and simple way to adopt Cartesian coordinate and orthogonal grid in the calculation for the turbulent flow in the furnace of utility boiler, whose geometrical boundaries are rather simple, it may not be a reasonable choice for the case of the TFB, because the disadvantageous deviations between grid lines and streamlines appear in the burner region of the furnace where the gradient of velocities is steep, and it leads to the serious NDE devastating the accuracy of the solution.

The body-fitted coordinate was adopted instead of Cartesian coordinate for modeling combustion in the TFB in the present study, while the physical domain was discretized in the manner to keep the grid lines aligned with the streamlines of fluid flow as well as the geometrical boundaries. These methods are justified as an effective way to reduce the NDE by satisfactory comparisons of computation and experiment.

Since the grid lines were arranged to fit both the flow patterns and the geometrical boundaries as a whole, the quality of the mesh featured by local non-smoothness and highly non-orthogonality was not so good that it may heighten the risk

of other numerical problems such as oscillation and divergence. The remedies of it in the present study were dependent on two special numerical techniques employed. The one is to smoothly dicretize metric factors by considering its geometrical property, and the other is to use secondary pressure correction method which is an enhancement to the projection method for accelerating the convergence rate of the solution of continuum equation in relatively poor curvilinear mesh.

A fully-elliptic numerical method for the solution of the full Navier-Stokes equations has been applied to the computational modeling of the isothermal flow in the TFB. The main features of the TFB flow appear to be captured correctly. The code and the grid systems provide a reliable bases for the combustion modeling in the utility furnace.

## References

Adrian, R. J. and Yao, C. S., 1987, "Power Spectra of Fluid Velocities Measured by Laser Doppler Velocimetry," *Experiments in Fluids*, Vol. 5, No. 1, pp. 17~28.

Choi, D. S., Choi, G. M. and Kim, D. J., 2002, "Spray Structures and Vaporizing Characteristics of a GDI Fuel Spray," *KSME International Journal*, Vol. 16, No. 7, pp. 999~1008.

Fan, J. R., Zha, X. D., Sun, P. and Cen, K. F., 2001, "Simulation of Ash Deposit in a Pulverized Coal-Fired Boiler," *Fuel*, Vol. 80, No. 5, pp. 645~654.

Ferziger, J. H. and Peric, M., 1995, *Computational Methods for Fluids Dynamics*, Springer Press.

Honnery, D. R. and Kent, J. H., 1989, "Furnace Flow Modeling: Physical and Computational," *J. of the Inst. of Energy*, Sep., pp. 169~177.

Kim, S. J. and Lee, C. M., 2002, "Numerical Investigation of Cross-Flow Around a Circular Cylinder at a Low-Reynolds Number Flow Under an Electromagnetic Force," *KSME International Journal*, Vol. 16, No. 3, pp. 363~375.

Luo, X. L., Boyd, R. K. and Kent, J. H., 1991, "Computational Investigation of Burnout in a Furnace Firing Pulverized Coal," *J. of Inst. of Energy*, Vol. 64, Dec., pp. 230~238.

Sandro, D. S., 2000, "Three Dimensional Modeling of Pulverized Coal Combustion in a 600 MW Corner Fired Boiler," *J. of Thermal Science*, Vol. 9. No. 4, pp. 376~380.

Smoot, L. D. and Pratt, D. T., 1979, *Pulverized-Coal Combustion and Gasification : Theory and Applications for Continuous Flow Processes*, Plenum Press, New York.

Su, J. T., 1999, *Experimental Study on T-Fired Boiler to Improve Cold Gas-Solid Flow in Furnace*, MEng. thesis, Tsinghua University.

Thompson, J. F., Warsi, Z. U. A. and Marstin, C. W., 1985, *Numerical Grid Generation*, North-Holland.

Wesseling, P., Segal, A., Kassels, C. G. M. and Bijl, H., 1998, "Computing Flows on General Two-Dimensional Nonsmooth Staggered Grids," *J. of Engineering Mathematics*, Vol. 34, No. 1-2, pp. 21~44.

Xu, H. and Zhang, C., 1998, "Study of the Effect of the Non-Orthogonality for Non-Staggered Grids," *Int. J. for Numer. Meth. Fluids*, Vol. 28, No. 9, pp. 1265~1280.

Yang, H. Q., Habchi, S. D. and Przekwas, A. J., 1994, "General Strong Conservation Formulation of Navier-Stokes Equations in Nonorthogonal Curvilinear Coordinates," *AIAA*, Vol. 32, No. 5, pp. 936~941